Online Data Supplements: Expanded Methods

I. *Boundary Conditions*:

Boundary conditions required for flow analysis were taken from a number of measured data bases since at present there is no single data source for all the required inputs.

Inlet, Outlet and Left Ventricle Pressures: P_A(t), P_V(t) and *LVP*(t) respectively, were taken from Hurst & Logue (6). The signals were modified for a specific heart rate by changing the diastolic time fraction (*DTF*, the period from minimal to maximal time derivative of *LVP* divided by the cardiac period (2)) taken from measured data (2). This modification is a close approximation for the complex relation between *DTF* and additional flow conditions (2). The signals amplitudes were modified as well: since the feed artery to the analyzed network is a distal (order 8) epicardial artery (rather than the coronary aortic outlet), the inlet pressure magnitude was scaled down to 100/70 mmHg in systole/diastole ((11); Fig. ODS-1A). Similarly, the outlet pressure (of the network's drain vein) was taken to follow aortic pressure waveform, but delayed so as to peak during aortic valve closure (16). The pressure magnitude was taken as 25/5 mmHg (11, 16).

Myocardial Activation (Fig. ODS-1B), lasting 0.26 seconds at endocardium (13), was taken to vary between 0 at diastole to 1 during peak activation. Depolarization was taken to initiate at the endocardium and propagate towards the epicardium at velocity of 50 cm/s (1) while repolarization propagates in the opposite direction at the same velocity.

*Sarcomere Stretch Ratio (*SSR*)* has been observed to be highly coupled to ventricular volume (54, 60). Thus, the ventricular volume waveform (6) was used for the *SSR* waveform, subject to 5% elongation from early to end diastole (15), and 16% shortening from end-diastole to end-systole (15, 17) as depicted in Fig. ODS-1C. Ventricular wall thickening was taken from measured data (4).

II. *Stochastic Reconstruction of the Coronary Network*

The reconstruction is based on morphometric data for porcine coronary vasculature (8-10). Briefly, arteries and veins are assigned orders ranging from 1 to 11 and from -1 to -12 in the arterial and venal networks, respectively. The terms “segment” and “element” are applied to a vessel portion between two vessel junctions and to a sequence of segments of the same order which are connected in series, respectively. Capillaries are also grouped, into those stemming from arterioles (Coa), venules (Cov) or other capillaries (Coo), and cross-connecting capillaries (Ccc).

Microvascular Network: The microvascular network reconstruction was carried out based on the morphometric data of Kassab et al. (8-10) regarding vessel lengths, vessel connectivity, and capillary branching pattern, and subject to two data-based constraints: i) the distance between arteriolar and venular domains (average of 510 μm, (8)), and ii) the ratio between arteriolar and venular segments (roughly 1 to 2, (9, 10)). One arteriole and two venules were located 510 μm apart. They were assigned order 1 and order -1, respectively. Arterial and venular capillaries (Coa and Cov) were attached to these corresponding vessels, according to connectivity data (9, 10) (see figure ODS-2A). The lengths of vessels were assigned according to the measured statistical data. Utilizing the branching patterns, Coo and Ccc were connected to the arterial and venular capillaries (Fig. ODS-2B). Subsequently, additional arterioles and venules were connected to the previously posed vessels, thus increasing the orders of the input and output vessels (Fig. ODS-2C). This process was iterated until the gaps between arteriolar and venular domains were bridged by capillaries, resulting in a network fed by one order 3 arteriole and two order –3 venules. In Tables ODS-1 to ODS-4 the reconstructed capillary branching pattern, arterial and connectivity matrices, and lengths and diameters of each order were compared to the measured data (8-10). A student T-test showed no statistically significant differences between the data and reconstructed network.

Arterial and Venous Trees: The order of arteries to first penetrate the cardiac wall ranges between 6 and 8 (7). Hence, the feeding artery was chosen to be an order 8. The number of generations arising from this arterial element, and the order of each segment in the tree were assigned based on the segment-to-element data (10). The order of the most distal segments was set to 4, thus matching the order of the reconstructed microvascular inlet arteriole. The length of each segment in the tree was assigned to fit the statistical data (8-10), while maintaining monotonic reduction of diameters along the element. The venous tree was reconstructed in a similar manner.

III. *The Deformation Gradient Tensors*

The deformation gradient $\boldsymbol{F}$ is determined by the mapping of coordinates between two loading configurations. Specifically, the transition between stress-free (*sf* subscript) and un-tethered (*unt*) configurations, combined with tissue incompressibility, leads to (5):

$$F^{v/m}_{sf\rightarrow unt} = \begin{bmatrix} \dfrac{\Theta_0^{v/m} r_{sf}^{v/m,in}}{\pi r_{unt}^{v/m,in} \Lambda_{unt,sf}^{v/m}} & 0 & 0 \\ 0 & \dfrac{\pi r_{unt}^{v/m,in}}{\Theta_0^{v/m} r_{sf}^{v/m,in}} & 0 \\ 0 & 0 & \Lambda_{unt,sf}^{v/m} \end{bmatrix} \qquad \text{(ODS 1)}$$

Here the superscript v/m denotes the specific cylinder: either vessel wall (v) or myocardium (m). Θ_0 is the opening angle (Fig. 3), r^{in} is the cylinder internal radius, and Λ is the axial stretch as defined in the main text. The deformation gradients associated with the transitions between un-tethered and unloaded (*unld*) configurations, and between unloaded and loaded configurations are:

$$F^{v/m}_{unt\rightarrow unld} = \begin{bmatrix} \dfrac{r_{unt}^{v/m,in}}{r_{unld}^{v/m,in} \Lambda_{unld,unt}^{v/m}} & 0 & 0 \\ 0 & \dfrac{r_{unld}^{v/m,in}}{r_{unt}^{v/m,in}} & 0 \\ 0 & 0 & \Lambda_{unld,unt}^{v/m} \end{bmatrix} \qquad \text{(ODS 2)}$$

$$F^{v/m}_{unld\rightarrow load} = \begin{bmatrix} \dfrac{r_{unld}^{v/m,in}}{r_{load}^{v/m,in} \lambda_z} & 0 & 0 \\ 0 & \dfrac{r_{load}^{v/m,in}}{r_{unld}^{v/m,in}} & 0 \\ 0 & 0 & \lambda_z \end{bmatrix} \qquad \text{(ODS 3)}$$

Here λ_z, the vessel dynamic axial stretch (see Appenix B), has the same level at both cylinders.

IV. ***Vessel and Myocardium Material laws***

Following previous studies, the description of the multiaxial material laws of vessel wall (19) and of the passive and active myocardium (12) are based on pseudostrain energy functions:

$$\begin{aligned} W_v &= \frac{C_{v,1}}{2}\left(\exp(Q_v)-1\right); \\ W_{m,pas} &= C_{m,1}\left(\exp(Q_m)-1\right); \\ W_{m,act} &= W_{m,pas} + C_{m,5} + C_{m,6}(I_1-3)(I_4-1) + C_{m,7}(I_1-3)^2 + C_{m,8}(I_4-1)^2 + C_{m,9}(I_1-3) + C_{m,10}(I_4-1) \end{aligned} \qquad (ODS\ 4)$$

where v, m pas and act subscripts denote vessel, myocardium passive and active, respectively, I_1 and I_4 are the first and fourth strain invariants respectively, and

$$\begin{aligned} Q_v &= C_{v,2}E_{\Theta\Theta}^2 + C_{v,3}E_{ZZ}^2 + C_{v,4}E_{RR}^2 + 2\left(C_{v,5}E_{\Theta\Theta}E_{ZZ} + C_{v,6}E_{ZZ}E_{RR} + C_{v,7}E_{\Theta\Theta}E_{RR}\right) \\ Q_m &= C_{m,2}(I_1-3)^2 + C_{m,3}(I_1-3)(I_4-1) + C_{m,4}(I_4-1)^2 \end{aligned} \qquad \text{(ODS 4a)}$$

E_{ii} are the components of the Green-Lagrange strain tensor, and $C_{i,j}$ are specimen-dependent parametrs which were previously estimated from data for vessel (19) and for myocardium (12).

V. ***Determining the Stress-Free Configuration***

To derive the stress-free configuration from the vessel cast (input) one, the internal and external radii of both cylinders (vessel wall and myocardium) at the three unknown configurations (unloaded, un-tethered and stress-free) are required. In addition to these 12 unknowns, 3 axial stretches need to be determined: the stretches of both vessel wall and myocardium due to closure of the opening angle ($\Lambda_{unt,sf}^{v}$ and $\Lambda_{unt,sf}^{m}$, respectively), and the myocardium stretch due to tethering, $\Lambda^{m}_{unld,unt}$. The vessels' tethering stretch $\Lambda^{v}_{unld,unt}$ is a measured input. Hence the total number of unknowns is 15.

The cast internal and external radii are known from the data (3, 8-10, 14, 18). Hence, in each unknown configuration and for each tissue (vessel and myocardium), for each given internal radius the incompressibility condition (Eq. B2 in Appendix B) yields the corresponding external one. Additionally, the assumption of common interface between cylinders at each of the above three configurations eliminates three more unknowns. Thus the number of unknowns is reduced from 15 to 6 (i.e., the vessel internal radii in stress-free, un-tethered and unloaded configurations; $r^{v,in}_{sf}$, $r^{v,in}_{unt}$ and $r^{v,in}_{unld}$, respectively, and the three unknown axial stretches listed above).

VI. *Computational Scheme for Flow Analysis*:

The solution of the ODE system described by Eqs. 1 and D1 in the main text must satisfy periodicity condition. This was fulfilled using the shooting method, i.e., after an initial guess of the intravascular pressure in each vessel, the numerical scheme was carried out for several cardiac cycles until solutions at consecutive cycles converged to within preset tolerance. This tolerance was set as follows: the maximum allowed pressure difference (at any of the vessels) between the beginning and the end of a cardiac cycle should be <0.1 mmHg. Numerical accuracy of the final solution was ascertained based on the criteria that the maximum difference between total flows into the feeding artery and out of its draining vein during a cardiac cycle was <5% of the total inflow.

REFERENCES

1. **Brugada J, Brugada P, Boersma L, Mont L, Kirchhof C, Wellens HJ, and Allessie MA.** On the mechanisms of ventricular tachycardia acceleration during programmed electrical stimulation. *Circulation* 83: 1621-1629, 1991.
2. **Fokkema DS, VanTeeffelen JW, Dekker S, Vergroesen I, Reitsma JB, and Spaan JA.** Diastolic time fraction as a determinant of subendocardial perfusion. *Am J Physiol Heart Circ Physiol* 288: H2450-2456, 2005.
3. **Guo X and Kassab GS.** Distribution of stress and strain along the porcine aorta and coronary arterial tree. *Am J Physiol Heart Circ Physiol* 286: H2361-2368, 2004.
4. **Hartley CJ, Latson LA, Michael LH, Seidel CL, Lewis RM, and Entman ML.** Doppler measurement of myocardial thickening with a single epicardial transducer. *Am J Physiol* 245: H1066-1072, 1983.
5. **Humphrey JD.** *Cardiovascular solid mechanics: cells, tissues, and organs*. New York: Springer, 2002.
6. **Hurst JW and Logue RB.** *The Heart, Arteries, and Veins*. New York: McGraw-Hill, 1970, p. 77.
7. **Kaimovitz B, Lanir Y, and Kassab GS.** Large-scale 3-D geometric reconstruction of the porcine coronary arterial vasculature based on detailed anatomical data. *Ann Biomed Eng* 33: 1517-1535, 2005.
8. **Kassab GS and Fung YC.** Topology and dimensions of pig coronary capillary network. *Am J Physiol* 267: H319-325, 1994.
9. **Kassab GS, Lin DH, and Fung YC.** Morphometry of pig coronary venous system. *Am J Physiol* 267: H2100-2113, 1994.
10. **Kassab GS, Rider CA, Tang NJ, and Fung YC.** Morphometry of pig coronary arterial trees. *Am J Physiol* 265: H350-365, 1993.
11. **Klassen GA, Armour JA, and Garner JB.** Coronary circulatory pressure gradients. *Can J Physiol Pharmacol* 65: 520-531, 1987.
12. **Lin DH and Yin FC.** A multiaxial constitutive law for mammalian left ventricular myocardium in steady-state barium contracture or tetanus. *J Biomech Eng* 120: 504-517, 1998.
13. **Nevo E and Lanir Y.** Parameter Estimation of Left Ventricle Performance. *Computers in Cardiology*, 1989, p. 251-254.
14. **Spaan JA.** *Coronary blood flow: mechanics, distribution, and control*. Dordrecht: Kluwer, 1991.
15. **Stevens C and Hunter PJ.** Sarcomere length changes in a 3D mathematical model of the pig ventricles. *Prog Biophys Mol Biol* 82: 229-241, 2003.
16. **Tillmanns H, Steinhausen M, Leinberger H, Thederan H, and Kubler W.** Pressure measurements in the terminal vascular bed of the epimyocardium of rats and cats. *Circ Res* 49: 1202-1211, 1981.
17. **Vis MA, Sipkema P, and Westerhof N.** Modeling pressure-area relations of coronary blood vessels embedded in cardiac muscle in diastole and systole. *Am J Physiol* 268: H2531-2543, 1995.
18. **Vis MA, Sipkema P, and Westerhof N.** Modeling pressure-flow relations in cardiac muscle in diastole and systole. *Am J Physiol* 272: H1516-1526, 1997.

19. **Wang C, Garcia M, Lu X, Lanir Y, and Kassab GS.** Three-dimensional mechanical properties of porcine coronary arteries: a validated two-layer model. *Am J Physiol Heart Circ Physiol* 291: H1200-1209, 2006.

FIGURE LEGENDS

Figure ODS-1: Model input boundary conditions. A) Left-ventricle (LVP (t), solid), feeding (P_A(t), dash) and draining (P_V(t), dots) pressure signals, under heart rate of 120 beats per minute. X-axis - time (in seconds), starting with endocardial activation. Y-axis - pressure (in mmHg, data taken from reference (6) and modified following (2, 11, 16)). B) Activation (13) at subepicardium (dash-dot) and subendocardium (solid). Time difference between the two signals is due to the finite velocity of activation propagation (1). C) Sarcomere stretch ratio (SSR(t), dash), reconstructed from LV volume (6), and myocardium wall thickening ((4), solid).

Figure ODS-2: A schematic of steps of the microvascular network reconstruction. A) One order 1 and two order -1 segments are located 510 μm apart, and Coa and Cov capillaries are added. B) Coo and Ccc capillaries are added while preserving branching pattern ratio. C) Arterioles and venules are added to enable bridging the gap between domains.

Table ODS-1: ***Capillary branching patterns***. *Comparison between reconstructed network and Kassab et al. (8) statistical data.*

Junction Pattern	Data	Reconstructed Network
T	0.2	0.19
Y	0.21	0.22
H	0.53	0.53
Hp	0.06	0.06

Table ODS-2: ***Reconstructed arteriolar connectivity matrix***. *Comparison between reconstructed network and Kassab et al. (10) statistical data (in brackets).*

Daughter Order	Mother Order		
	1	2	3
0	3 (3.2)	0 (0.67)	0 (0.15)
1	0 (0.14)	2 (2.04)	1 (0.63)
2		0 (0.09)	3 (2.24)
3			0 (0.07)

Table ODS-3: ***Reconstructed venular connectivity matrix***. *Comparison between reconstructed network and Kassab et al. (9) statistical data (in brackets).*

Daughter Order	Mother Order		
	-1	-2	-3
0	2.7 (2.56)	0 (0.42)	0 (0.35)
-1	0 (0.105)	2 (2.47)	1 (0.77)
-2		0 (0.11)	3 (2.44)
-3			0 (0.07)

Table ODS-4: The *Vessels' lengths and diameters*: *Comparison between reconstructed microvascular network and data (8-10). Asterisks stand for arterioles' diameters which were altered according to their intramural location (see Appendix B).*

Vessel Type	Data		Reconstructed Network		p-value (reconstructed vs. data)
	n	Mean (SD)	n	Mean (SD)	
	Segment Length (microns)				
Order 3	177	72 (49)	3	70.4 (33.7)	0.47
Order 2	326	72 (45)	3	75.5 (35.5)	0.44
Order 1	506	56 (38)	14	58.8 (39.0)	0.40
Order -1	251	51 (41)	19	49.5 (29.0)	0.42
Order -2	313	56 (41)	8	55.4 (33.4)	0.48
Order -3	263	63 (43)	4	66.5 (34.1)	0.43
Coa	222	52 (32.3)	21	48.5 (30.9)	0.31
Cov	34	45 (30.5)	33	43.7 (19.8)	0.42
Ccc	161	21.1 (15.5)	20	20.2 (6.0)	0.31
Coo	86	54.5 (43)	49	56.8 (25.6)	0.35
Segment Diameter (microns)					
Order 3	266	18.7 (2.6)	3	18.4 (1.0)*	0.34
Order 2	539	13.0 (1.7)	3	13.2 (0.8)*	0.38
Order 1	835	9.2 (0.94)	14	9.1 (0.5)*	0.19
Order -1	251	10.8 (1.7)	19	11.1 (1.0)	0.14
Order -2	313	17.6 (3.0)	8	17.1 (1.8)	0.24
Order -3	263	30 (4.3)	4	29.4 (3.9)	0.38
Coa	222	6.2 (1.1)	21	6.1 (0.6)	0.35
Cov	34	7.0 (1.2)	33	6.9 (0.7)	0.36
Ccc	161	5.5 (1.2)	20	5.5 (0.8)	0.44
Coo	86	5.7 (1.4)	49	5.6 (0.7)	0.22

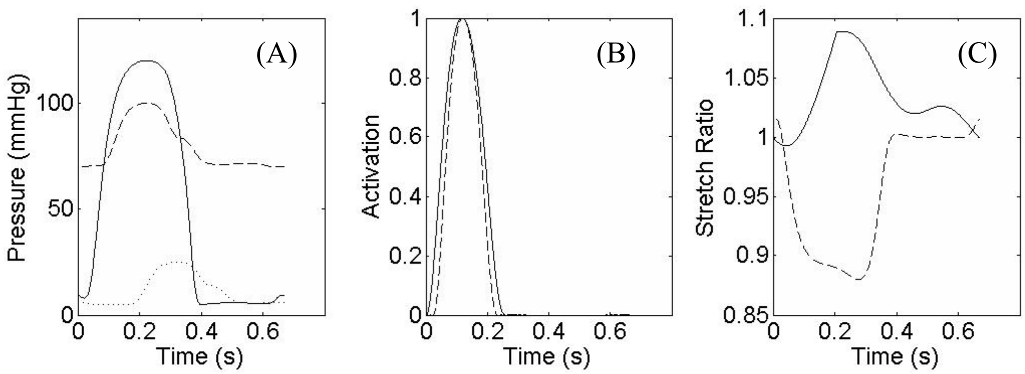

(A)
Pressure (mmHg)
Time (s)
(B)
Activation
Time (s)
(C)
Stretch Ratio
Time (s)

Figure ODS-1

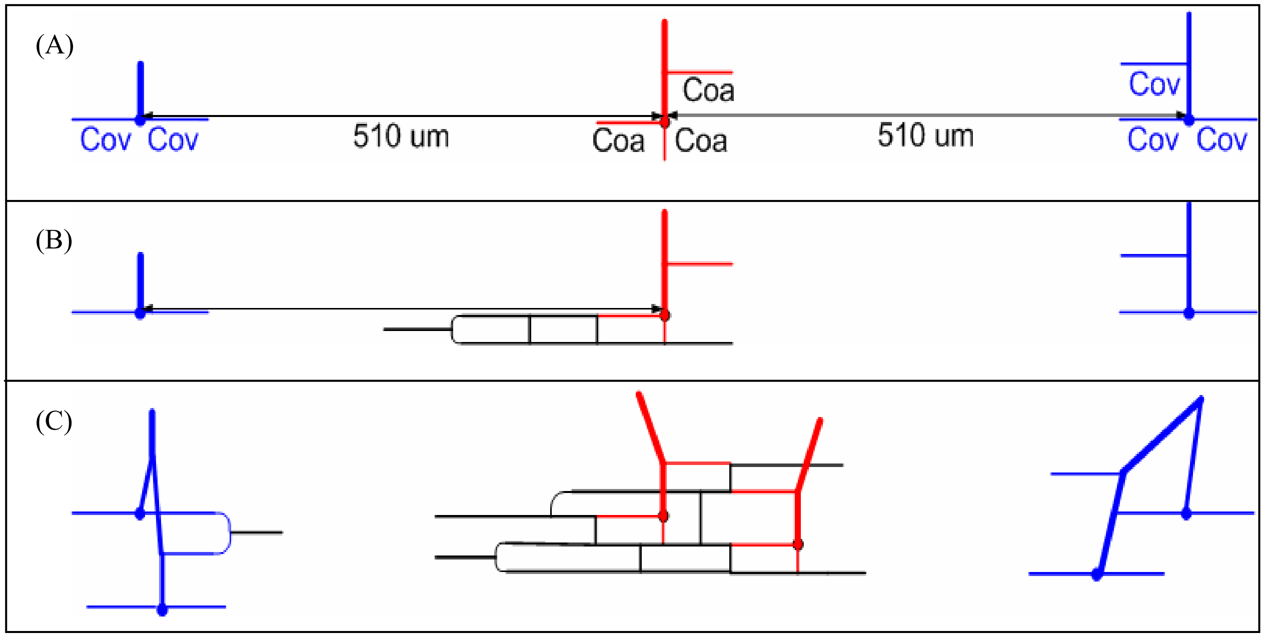

Figure ODS-2